Modeling and Simulation of Vitrimers

Alessandro Perego, Harsh Pandya, and Fardin Khabaz

Abstract The healing response in self-healing materials is regulated by the rates of three distinct stages: actuation, transport, and repair. The healing efficiency is dictated by delicately balancing the rate of damage versus the rate of healing. The material damage rate is determined by the frequency of strain rate, loading, and stress amplitude. However, by changing the reaction kinetics through temperature or concentration the healing rate can be designed to specific damage modes. Vitrimers are a particular subcategory of intrinsic self-healing materials that flow at temperatures higher than the topology freezing temperature and show thermoset-like behavior at low temperatures. Vitrimer chemistry is an excellent way to combine the favorable mechanical properties of covalently crosslinked thermosets with full recyclability and create intrinsic self-healing materials without needing a healing agent. Recently, several theoretical frameworks, coarse-grained particle dynamics simulations, and finite element analysis (FEA) have been used to probe the thermodynamics, dynamics, rheology, and mechanics of these transient networks. Particle-based dynamic simulations have successfully produced key features of vitrimers, rubbery plateau, and terminal modulus behaviors. On a continuum level, constitutive equations have been developed to study the effect of the kinetics of the bond exchange on the macroscopic material response. In this chapter, the recent advances in the modeling aspect of vitrimers ranging from particles-based simulation techniques to FEA are reviewed.

Keywords Vitrimers · Thermoset · Rheology · Mechanics · Molecular simulations · Finite element analysis

A. Perego · H. Pandya · F. Khabaz (✉)
School of Polymer Science and Polymer Engineering, The University of Akron, Akron, OH 44325, USA
e-mail: fkhabaz@uakron.edu

F. Khabaz
Department of Chemical, Biomolecular, and Corrosion Engineering, The University of Akron, Akron, OH 44325, USA

N. Hameed et al. (eds.), *Multifunctional Epoxy Resins*, Engineering Materials,
https://doi.org/10.1007/978-981-19-6038-3_8

1 Introduction

The aim of self-healing process is to achieve equilibrium in the material by carefully adjusting the rate of healing and the rate of damage [1]. Self-healing materials are usually classified into three main categories: *capsule based*, *vascular*, and *intrinsic* [2]. This classification is based on the mechanism used to isolate the healing functionality of the material. According to the type of sequestration used, it is possible to control how many times the material can be healed, the damaged volume available for healing, and the kinetics of the recovery rate.

Capsule-based self-healing materials sequester the healing agent in discrete capsules. When the induced damage ruptures these capsules, the release and reaction of the healing agent initiate the self-healing process [3]. In *vascular self-healing* materials, the self-healing materials are stored in capillaries. These networks may be interconnected in one, two, or three dimensions until damage triggers the self-healing process [3]. After the rupture of the capillaries and subsequent release of the healing agent, the material can be replenished with the healing agent, thus allowing for multiple local healing events to occur.

There is no healing agent in *intrinsic* self-healing materials, but they possess self-healing functionalities directly embedded in their chemical structure. These functionalities are usually initiated by damage or an external stimulus. For polymeric materials, this self-healing process can be achieved by phenomena such as reversible polymerization, hydrogen bonding, ionic interactions, and reversible bond exchange reactions [3]. Each of these reactions is reversible, and thus, multiple healing events can occur for intrinsic self-healing materials [1].

Generally, polymers are divided into thermoplastics, in which polymer chains are not chemically attached, and thermosets, in which chains are permanently crosslinked [4–9]. Thermoplastic materials show flow behavior similar to a viscoelastic liquid when heated [8, 10, 11] that allowing these materials to be re-processable [12]. However, the molecular topology changes directly result in weak solvent resistance and poor mechanical properties [5, 13]. The diffusion of polymer chains in thermoset materials is suppressed since the network is crosslinked [14], thus making the thermosets suitable for applications that require strong mechanical properties such as coatings, electronics, and structural applications [12, 15]. However, as thermosets present a theoretically infinite rubbery plateau when heated above the glass transition temperature (T_g) due to the connectivity of the network; thus these materials cannot be reprocessed after they are crosslinked [16]. Considering the latter limitation, i.e., difficulty in reprocessing thermosets, these materials provide a significant challenge for recycling polymers (see Fig. 1) [16–18].

Several attempts have been made to implement non-covalent bonds as crosslinkers in thermoset, including hydrogen bonds [19, 20], π–π stacking [21], and metal–ligand bonds. However, due to the weaker energy of the non-covalent bond interactions [22], these materials show poor mechanical properties compared to commercially available thermosets. A more promising approach introduces dynamic covalent bonding into thermosetting materials, creating what is commonly known

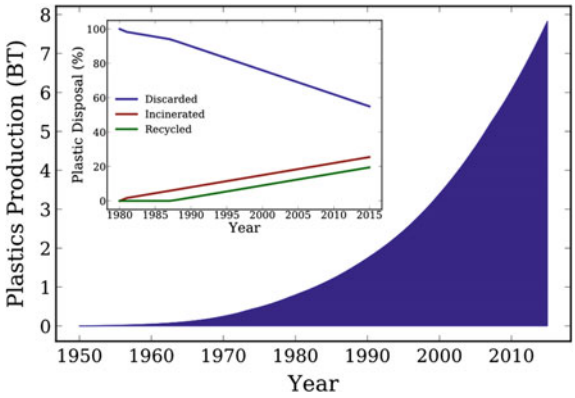

Fig. 1 Cumulative global plastic production from 1950 to 2015. Inset: Global plastic waste disposal from 1980 to 2015. As it emerges from the data, as of 2015, only, ~ 19% of the total plastic produced is recycled successfully [18]. The data in the figure are obtained from Geyer, Jambeck, Lavender Law; Production, use, and the fate of all plastics ever made; Sci. Adv.; 2017; American Association for the Advancement of Science

as covalent adaptive networks (CANs) [4–6, 23]. Depending on the chemistry of the bond exchange mechanism, CANs can be further classified as either *associative* or *dissociative* [24, 25]. *Associative* CANs rely on associative exchange mechanisms in which the original crosslink is only broken when a new covalent bond to another position has been formed [4–6, 25–28]. As a result, upon heating, there is no depolymerization and the crosslink density of these networks also remains constant [29, 30]. Despite displaying promising rheological properties, the timescale associated with the bond exchange reaction of these systems remains restricted due to the radical nature of the catalyst used [25].

In 2011, Leibler and coworkers [27] proposed a unique approach to *associative* CANs by adding a suitable transesterification catalyst to an epoxy/acid or epoxy/anhydride polyester-based network. These materials are named vitrimers, and they show a gradual decrease in the viscosity of the system upon heating following an Arrhenius law with an activation energy of ~ 80 k J/mol K, similar to inorganic materials such as silica [4, 31, 32]. This characteristic viscosity behavior enables vitrimers to be processed in wide temperature ranges without any potential loss in network integrity [6]. Also, unlike *dissociative* CANs, vitrimers show solvent resistance [25]. Additionally, rheology and birefringence experiments show that these networks can rapidly relax stress and display great malleability [5, 27, 33, 34], weldability [25, 26], and shape memory [35–37]. Leibler and coworkers proposed a new class chemical route using the metathesis of dioxaborolanes to create vitrimers using polymethyl methacrylate, polystyrene, and high-density polyethylene as backbone chains of the network. These vitrimers can be processed several times via extrusion or injection molding [6]. Hence, there is a possibility for repair assembly and alloying incompatible polymers, and most importantly, providing new routes for recycling thermosetting plastics.

Two transition temperatures describe the thermodynamics and kinetics of vitrimers [6, 28, 38–40]: (1) the glass transition temperature, T_g, which is common in amorphous polymeric materials [11] and (2) the topology freezing temperature, T_v, which shows the transition from viscoelastic solid to viscous liquid behavior and often appears at a temperature above the T_g. At this temperature, the timescale of the topological change becomes slow upon cooling, and the network rearrangement becomes sluggish. In experiments, this transition is selected at a temperature where the value of shear viscosity reaches 10^{12} Pa·s [4, 11, 41]. Different factors, such as the chemistry of the monomer and crosslinker, number density of crosslinker, loading of catalyst, quenching rate, and the density of exchangeable bonds, dictate the viscoelastic properties of vitrimers [4]. Ideally, these materials should be designed such that they behave like a thermoset network in practical applications and flow like a viscous liquid during processing at high temperatures without loss of network integrity. It has been suggested that it might be possible to determine the T_v from volumetric data similar to the glass transition, but as of now, due to the instrument limitations, the detection of T_v from direct experimental measurements is a challenging task [5].

Atomistically detailed molecular dynamics (MD) simulations have been successfully used to study the bonds exchange reactions at the interface during stretching and welding processes in polymeric materials. However, the high computational cost of all-atom simulations poses a serious limitation on the choice of the system size and on the time scale accessible, making it challenging to capture the complex dynamics of *associative* CANs such as vitrimers accurately. A possible way to extend the molecular modeling time scale and bridge it with experimental procedures is to apply coarse-graining. This technique allows representing a system by a reduced (in comparison with an all-atoms simulation) number of degrees of freedom. The simulation of a coarse-grained (CG) system is less computationally expensive than the same system in all-atom representations due to reduced degrees of freedom and elimination of the fine interaction details. This results in an increase of orders of magnitude in the simulated time and length scales. In the case of vitrimers, there is an urgent need to predict their viscoelastic properties and dynamics in a relevant timescale to experiments [28].

Continuum models also show quantitative agreement between the stress–strain behavior and stress relaxation modulus and experimental results [42]. Recently, a patchy particle model implementing a three-body potential similar to the Stillinger–Weber force field was proposed to investigate the dynamics of the vitrimers [40]. This model was used to study the phase separation [40], self and collective dynamics of the vitrimer system formed using the patchy colloidal particles [40, 43–46]. A recent study [47] on aging dissociating polymers based on a coarse-grained bead-spring method and Langevin dynamics concluded that the aging is due to the dissociation of small clusters of sticky monomers and transformation of the small clusters to a large one. In our recent study [48, 49], we have combined molecular dynamics (MD) and Monte Carlo (MC) simulations to predict the dynamics and rheology of a model vitrimer and compared its properties with a permanently crosslinked one. Our

results show that a simple bond exchange protocol accompanied with an appropriate coarse-graining level generates the essential characteristics of vitrimers.

In this chapter, we review the available simulation methods and summarize the results on the mechanical and rheological properties of these novel polymeric systems. We close this chapter with a summary of the models and an outlook on the computational techniques.

2 Simulation and Modeling Techniques and Theoretical Frameworks

2.1 Particle-Based Models

Generally, in these types of simulations, a collection of a few atoms is considered one particle, or bead, with an appropriate nonbonded and bonded energy that governs the force field between all the beads in the system tuned to capture roughly the effect of polymer chemistry. The trajectories of particles are predicted using appropriate equations of motion, and using the principles of statistical mechanics, the properties of the system are predicted as a function of the simulation time.

2.1.1 Patchy Particles and Three-Body Potential

Using a coarse-grained model, Smallenburg et al. [50] studied the phase behavior of vitrimers in a solvent phase. The study used event-driven molecular dynamic simulations (EDMD) and Wertheim's theory for free energy calculations for simulating vitrimers [51]. The model system presented a mixture of two types of patchy particles, namely particles A and B with $f_A = 4$ and $f_B = 2$, where f denotes the number of attractive patches on the particle surface arranged in tetrahedral and polar geometries, respectively. The particles were designed based on the Kern-Frenkel model [52]. The size of the patches was defined based on their opening angle θ_m with $\cos\theta_m = 0.8$. The patches can only be involved in one bond at a time, and that is, multiple bonding partners are available. This type of associative bond exchange in the system satisfies the requirement for a vitrimer network. The interactions in the model system were considered as a combination of the repulsive potential between beads of diameter σ with a mass of m and attractive interaction between the surface particle patches. The bonding between patches could not exceed the maximum bond length of 1.2σ with the condition that the vector linking the centers of any two particles passes through at least one patch on each particle. The rate of bond switching was controlled according to the system by varying the temperature and/or the catalyst load. Using the autocorrelation of the off-diagonal elements of the stress tensor, the dimensionless shear viscosity $\eta\beta\sigma^3 / \tau$, where $\beta = 1 / k_B T$, with k_B is the Boltzmann constant, and τ is

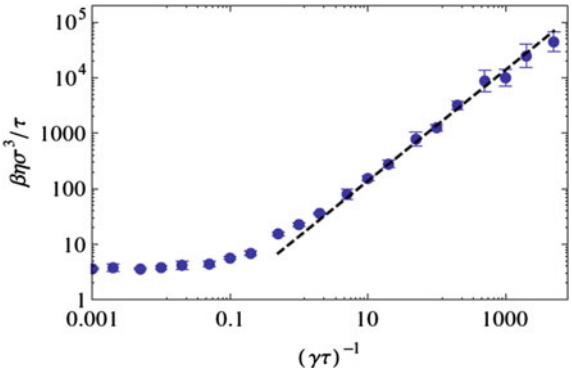

Fig. 2 Dimensionless shear viscosity $\beta\eta\sigma^3/\tau$ as a function of the average time interval between bond switching events. The dashed line indicates an Arrhenius fit (slope = 1). The viscosities were calculated at the composition of $x = 0.25$ (where x is the ratio of the number of patches of A to the total number of patches (A + B)), and number density of $\rho\sigma^3 = 0.35$, where σ is the diameter of the particle, well away from the area where phase separation occurs. τ is the units of time and is defined as $\tau \equiv \sqrt{\beta m\sigma^2}$, where m is the mass of particle and $\beta = 1/k_BT$, with k_B is the Boltzmann constant. The figure is obtained from Smallenburg, Leibler, Sciortino; Patchy Particle Model for Vitrimers; Phys. Rev. Lett.; 2013; American Physical Society

the units of time and is defined as $\tau \equiv \sqrt{\beta m\sigma^2}$, was obtained at different average times between bond switching events, as seen in Fig. 2 (note that the frequency of the bond exchange γ scales with $\exp(-\varepsilon_a/k_BT)$, where ε_a is the activation energy). At small time intervals, when bond switching occurs fast, the viscosity of the system is constant, while at $(\gamma\tau)^{-1} \gg 1$, a linear relationship with $(\gamma\tau)^{-1}$ is seen for the viscosity, and consequently, an Arrhenius-like behavior of the viscosity is observed.

Another type of coarse-grained simulation for polymers often is performed using the bead-spring model [53], where beads interact using a Weeks-Chandler-Anderson (WCA) potential [54]. The monomer bond exchange was implemented using the WCA potential for nonbonded particles, the harmonic potential for bonded particles, and a three-body potential based on the Stillinger–Weber potential. The dynamics of the transient networks are predicted as a function of time. A similar method incorporating a three-body potential based on the Stillinger–Weber potential [55] was proposed to study the self and collective dynamics of vitrimers [46]. These two types of dynamics were quantified using the intermediate scattering functions (ISFs), and a two-step relaxation was observed for the self and collective part of the ISF.

Eight-arm star-shaped polymers with carboxyl and hydroxyl end groups, respectively, were simulated using the latter method [56]. The underlying idea behind the three-body potential is based on the addition of a repulsive potential based on interactions three-body interactions between *i-j* and *i-k* particles. It also involves a parameter λ used to interpolate between a bong swapping and permanently connected systems. When the value of $\lambda >> 1$, a system with an infinitely long bond lifetime is simulated. When $\lambda = 1$, the additional potential energy gain associated with the

formation of the double bond is compensated by the value of the three-body potential. The systems were divided into a defect free mixture (DFM), which was a mixture of star polymers with either only groups A or B as the end groups, and a defect allowing mixture (DAM), which consisted of star polymers with seven arms ending with group A and one with group B. After forming bonds in the DAM, the A-type ends were free to initiate bond swapping. Both systems were equilibrated in periodic cubic boxes with a packing fraction of 0.3. For the stress relaxation calculations, the Green–Kubo method [57] was used in a constant number of particles, volume, and temperature (NVT) ensemble to calculate the stress $\sigma(t)$ autocorrelation function.

In Fig. 3a and b, the stress relaxation of DFM and DAM systems as a function of the time at different energy barrier values is plotted. For times shorter than that elastic plateau timescale, the chain motion dominates stress relaxation. When the energy barrier of the bond swap is high, the topology of the network remains unchanged, and the elastic plateau extends beyond the time scale for simulation. However, for the case with no energy barrier, which enables bond swapping, there is a second relaxation observed, as shown in Fig. 3. This is a characteristic feature of transient networks such as vitrimers. The stress relaxation time in this scenario was about 20 μs. In the case of DAM, the solid plateau is achieved by the fixed network, while the transient networks result in stress relaxation over shorter timescales. The stress relaxation was 10 times faster with the stress relaxation time of 2 μs which essentially shows the DAM networks behave like a viscous liquid. In the inset of Fig. 3b, the comparison between the stress relaxation modulus in these two networks is presented, and as seen, the improved stress relaxation is a result of the defects when the number of the bond swaps was the same for both. It was indicated that a defect loop was formed every time an intra-star bond was experiencing stress which led to dissipation, and given that the swap rates were the same for both networks, it was concluded that the defect loops acted like highways for stress relaxation. It was further hypothesized that these loop defects could be used to speed up the stress relaxation process, enhance properties of self-healing, and make the material more malleable and recyclable.

2.1.2 Hybrid Molecular Dynamics–Monte Carlo Technique

Recently, we proposed a hybrid molecular dynamics–Monte Carlo (MD–MC) method to describe the dynamics and linear rheology of vitrimers at different temperatures [49, 58]. Pant and Theodorou devised an algorithm based on the connectivity-altering atomistic Monte Carlo (MC) approach to accelerate the equilibrium of condensed phases of long-chain systems with a range of chain architectures [58, 59]. Following their work, similar MD–MC algorithms have been implemented to examine materials with reversible bonds, such as thermoreversible gels, supramolecular polymer, and telechelic polymers [47, 60–62]. Based on those methods, it is proposed an adaptation of the MD–MC algorithm that can be used for reproducing the bond exchange reactions in associative CANs, specifically in vitrimers.

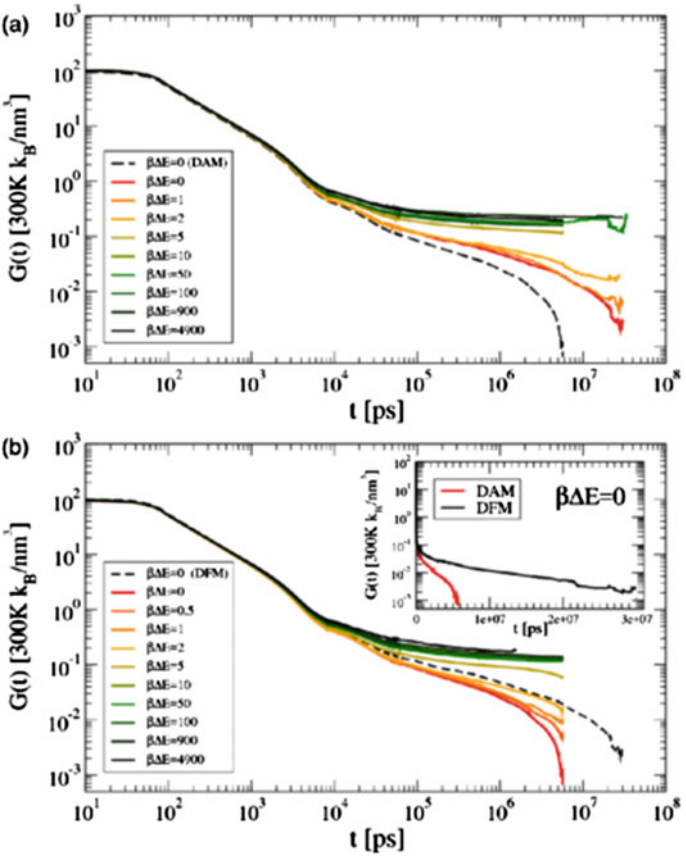

Fig. 3 **a** Stress relaxation for DFM for a range of energy barrier values. **b** Comparison between the DAM and DFM stress relaxation values. The figure is obtained from Ciarella, Sciortino, Ellenbroek; Dynamics of Vitrimers: Defects as a Highway to Stress Relaxation; Phys. Rev. Lett.; 2018; American Physical Society

To explain how the algorithm works, let us suppose we have a system consisting of a few polymers chains such as the one depicted in Fig. 4. These polymers are made of n monomers units, but only one terminal monomer can react to form additional bonds with other chains. At $t = t_0$, two polymer chains are covalently bonded with each other. At every user-defined time step, each reactive monomer is sampled to find a possible new monomer for the bond exchange. Assuming that (i, j) and (k,l) are two exchangeable bonds pairs, for a monomer found at a distance r defined by the user, the energy change $\Delta\tilde{U}_{\text{Exchange}}$:

$$\Delta\tilde{U}_{\text{Exchange}} = \alpha\Big(\tilde{U}_{\text{New}}(i,l) + \tilde{U}_{\text{New}}(j,k) - \tilde{U}_{\text{Old}}(i,j) - \tilde{U}_{\text{Old}}(k,l)\Big), \qquad (1)$$

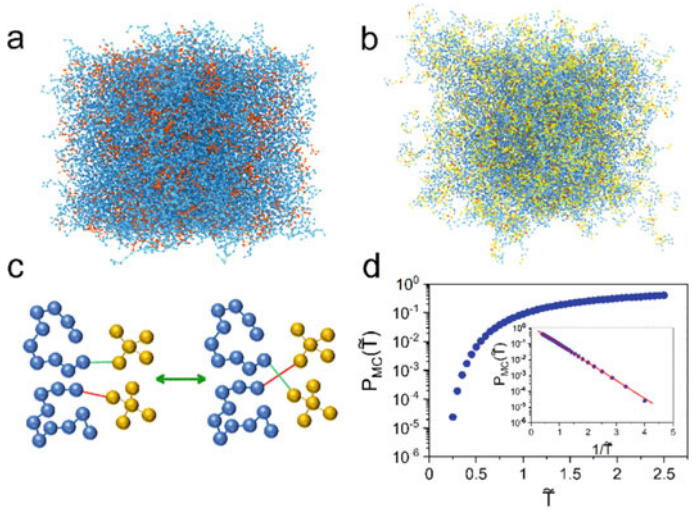

Fig. 4 Mixture of 10-mer chains (blue) with crosslinkers (orange) before **a** and after **b** crosslinking the network (yellow correspond to the reacted beads). **c** Bond exchange reaction schematic. Red and green colors are used to represent the exchangeable bonds. **d** Probability of an exchange reaction $P_{\mathrm{MC}}\left(\tilde{T}\right)$ as a function of temperature $\tilde{T}$ in vitrimers. The red line in the inset shows the exponential fit to the data. The figure is obtained from Perego, Khabaz; Volumetric and Rheological Properties of Vitrimers: A Hybrid Molecular Dynamics and Monte Carlo Simulation Study; Macromolecules; 2020; American Chemical Society

can be computed. If $\Delta\tilde{U}_{\mathrm{Exchange}} \leq 0$, the new configuration will be accepted, and if $\Delta\tilde{U}_{\mathrm{Exchange}} > 0$, the move is accepted based on the Boltzmann acceptance criterion [63, 64]. The α parameter is a dimensionless factor that is introduced to mimic the effect of a bond exchange reaction assisted by a catalyst. The polymer network is simulated using the well-established CG framework introduced by Kramer and Grest, in which the polymer chains are modeled as spherical beads connected by springs [53]. Within an atomistic model, each bead corresponds to multiple monomer units. All units are normalized in terms of reduced Lennard–Jones (LJ) parameters: length $= \sigma$, energy $= \epsilon$, and time $= (m\sigma^2/\epsilon)^{1/2}$ with the bead mass of m. The nonbonded interaction is calculated using a shifted and truncated Lennard–Jones (LJ) potential defined as:

$$\tilde{U}_{\mathrm{LJ}}(\tilde{r}) = \begin{cases} 4\left[\left(\frac{1}{\tilde{r}}\right)^{12} - \left(\frac{1}{\tilde{r}}\right)^{6} - \left(\frac{1}{\tilde{r}_c}\right)^{12} + \left(\frac{1}{\tilde{r}_c}\right)^{6}\right] & \text{for } \tilde{r}_c \leq 2.5 \\ 0 & \text{for } \tilde{r}_c > 2.5 \end{cases}, \tag{2}$$

where r represents the distance between two beads and r_c represents the cut-off distance. Throughout the simulation, the chain structure is maintained numerically such that the nearest-neighbor beads along the chain are permanently bonded. These permanent bonds are anharmonic, finitely extensible, nonlinear, and described by an

elastic (FENE) potential:

$$\tilde{U}_{\text{Bond}}(\tilde{r}) = -\frac{K}{2}\tilde{r}_0^2 \ln\left[1 - \left(\frac{\tilde{r}}{\tilde{r}_0}\right)^2\right], \tag{3}$$

An appropriate choice of parameter consists of setting $R_{\max} = 1.5\sigma$, and k $= 30\epsilon/\sigma$ as it avoids the possibility of chains passing through one another [64–66].

The initial crosslink network is constructed using a tetrafunctional crosslinker consisting of five beads with the four end beads being reactive and a linear molecule with two reactive terminal beads. Reactions are only allowed between the reactive beads. The simulated annealing polymerization technique [67, 68] is used to connect the tetrafunctional molecules with the linear ones and build the final crosslinked structure. In Fig. 4a–c, the simulation box before and after reaction and the schematics of the monomer and crosslinker are shown, respectively. The relaxation and quenching simulations from a high temperature of 2.0 to 0.1 were performed in an isothermal–isobaric ensemble with a pressure of zero. The probability of the bond exchange between the crosslinker junctions $P_{\text{MC}}\left(\tilde{T}\right)$ is determined and plotted in Fig. 4d at each temperature. As seen in the figure, $P_{\text{MC}}\left(\tilde{T}\right)$ follows an Arrhenius-like temperature dependence.

The volumetric properties of the model thermoset and vitrimer networks were quantified by determining the specific volume, coefficient of thermal expansion, and glass transition temperature. In Fig. 5a, the specific volume of the model systems is plotted as a function of temperature. Both thermoset and vitrimer systems show similar $\tilde{T}_g$ values, which are expected since the bond exchanges become relevant only at high temperatures (see Fig. 4d for the probability of the bond exchange). At temperatures higher than $\tilde{T}_g$, the specific volume of vitrimer becomes larger than that of thermoset that is more visible in the dimensionless excess volume $\tilde{V}^E = \left(\tilde{V}_{\text{vitrimer}} - \tilde{V}_{\text{thermoset}}\right) \Big/ \tilde{V}_{\text{thermoset}}$ in the inset of Fig. 5a. We plot the coefficient of thermal expansion $\tilde{\alpha} \cdot \left(\tilde{\alpha} = \left(\partial V \Big/ \partial T\right)_p \Big/ V\right)$ in Fig. 5b for these two systems. Both thermoset and vitrimer networks show a discontinuous behavior for $\tilde{\alpha}$ at $\tilde{T}_g$. At $\tilde{T} > \tilde{T}_g$ the thermoset shows a constant value of $\tilde{\alpha}$; on the other hand, a local minimum point at $\tilde{T} \simeq 0.87$ for the values of $\tilde{\alpha}$ is seen in the model vitrimer.

The dynamics of the crosslinkers in the model systems were determined by calculating the mean squared displacement (MSD) $\left\langle \Delta\tilde{r}^2(\tilde{t}) \right\rangle$ at different temperatures. As seen in Fig. 6a, at temperatures below the glass transition temperature, both systems show similar mobility. As the temperature steadily increases and exceeds the $\tilde{T}_g$, the vitrimer shows higher mobility. At higher temperatures (see Fig. 6c and d), the crosslinkers show a nearly diffusive behavior, while the motion of the crosslinker in the thermoset network is impeded due to the existence of permanent bonds.

Using the hybrid MD–MC method [58], the rheology of the networks can also be determined. We refer readers to our study on the volumetric, dynamics, and rheology of the vitrimers for detailed discussion. Here, we focus on the primary outcomes of

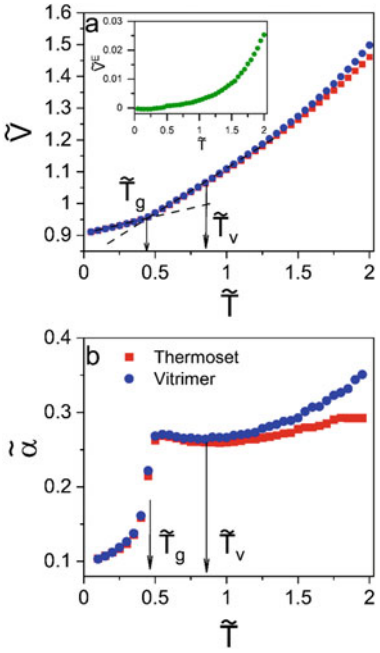

Fig. 5 **a** The specific volume $\tilde{V}$ and **b** thermal expansion coefficient $\tilde{\alpha}$ as a function of reduced temperature $\tilde{T}$ for both thermoset and vitrimer. Inset in **a:** The rescaled excess volume $\tilde{V}^E = \left(\tilde{V}_{\text{vitrimer}} - \tilde{V}_{\text{thermoset}}\right) \Big/ \tilde{V}_{\text{thermoset}}$ as a function of the temperature. At every temperature, the uncertainty for each data point is about 0.1% of the magnitude of the specific volume (smaller than symbol size). The intersection of the fitted lines (dashed lines in **a**) in the rubbery and glassy regions corresponds to the glass transition temperature $\tilde{T}_g$ of the system. The figure is obtained from Perego, Khabaz; Volumetric and Rheological Properties of Vitrimers: A Hybrid Molecular Dynamics and Monte Carlo Simulation Study; Macromolecules; 2020; American Chemical Society

the rheological simulations that are (1) applicability of the time–temperature superposition (TTS) principle to extend the simulation timescale and (2) Arrhenius-like temperature dependence of the viscosity of vitrimer. The linear viscoelastic moduli of the thermoset and vitrimer were determined using the NEMD method [69] by incorporating the SLLOD equations of motion [70] at different frequencies and temperatures. The TTS principle is used to collapse data onto master curves at a reference temperature of $\tilde{T}_0 = 0.6$. In Fig. 7a, the elastic modulus of the thermoset network is plotted against the oscillation frequency. The thermoset network exhibits a rubbery modulus at low frequencies and a glassy response after a Rouse-like transition regime. The vitrimer model essentially behaves the same way as the thermoset at intermediate and high frequencies, given that the deformation rate is larger than the bond exchange rate, as seen in Fig. 7b. On the other hand, at lower frequencies, the elastic modulus of the vitrimer appears to show a liquid-like behavior (or so-called terminal regime). The latter observation is due to the fast timescale of the bond exchange in that deformation regime, which corresponds to long times. Both

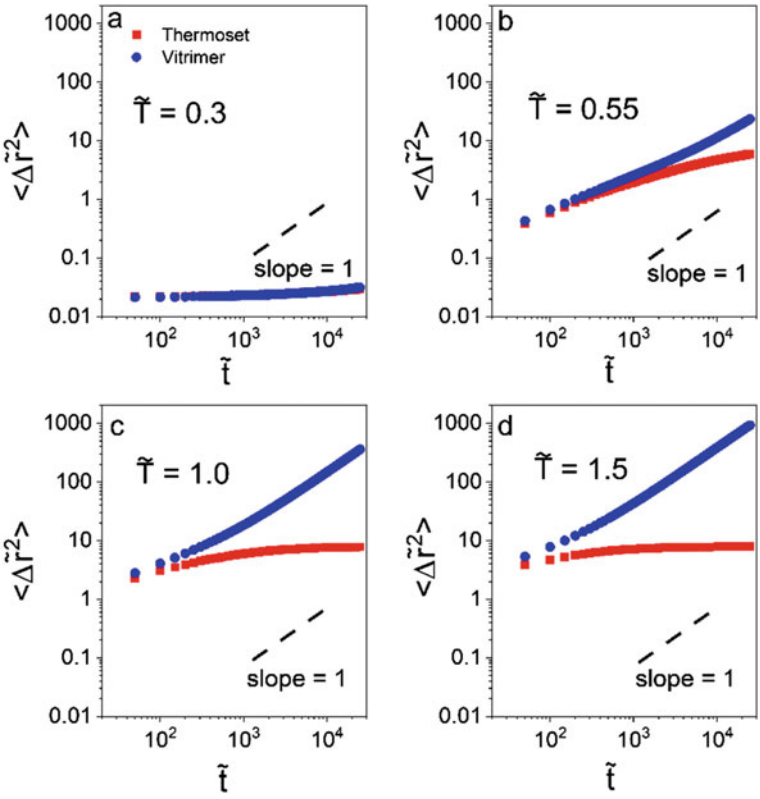

Fig. 6 Mean-squared displacement (MSD) $\left\langle \Delta\tilde{r}^2(\tilde{t}) \right\rangle$ of the crosslinking beads (reactive beads that can participate in the exchangeable reaction) in thermoset and vitrimer at **a** $\tilde{T} = 0.3$, **b** $\tilde{T} = 0.55$, **c** $\tilde{T} = 1.0$, and **d** $\tilde{T} = 1.5$. The diffusive motion is shown by the dashed line, which has a slope of unity on the log–log scale. The figure is obtained from Perego, Khabaz; Volumetric and Rheological Properties of Vitrimers: A Hybrid Molecular Dynamics and Monte Carlo Simulation Study; Macromolecules; 2020; American Chemical Society

viscous moduli of thermoset and vitrimer show the same behavior (see Fig. 7c and d). We expect to observe the difference in the viscous moduli at lower frequencies which are not accessible in the current simulations. Note that the shift factors used to collapse rheological data follow Williams-Landel-Ferry (WLF) equation for the thermoset network, while this temperature dependence for the vitrimer model becomes more complex (see Fig. 8). The temperature dependence of the shift factor follows a combination of the WLF equation at low temperatures and Arrhenius behavior at high temperatures in model vitrimer. The intersecting temperature between these two regimes corresponds to a temperature of 0.85, which is very close to the temperature that coefficient of thermal expansion shows a local minimum. In addition, the zero-shear viscosity of the vitrimer model shows an Arrhenius-like form which validates the model consistency with the temperature dependence of shift factors.

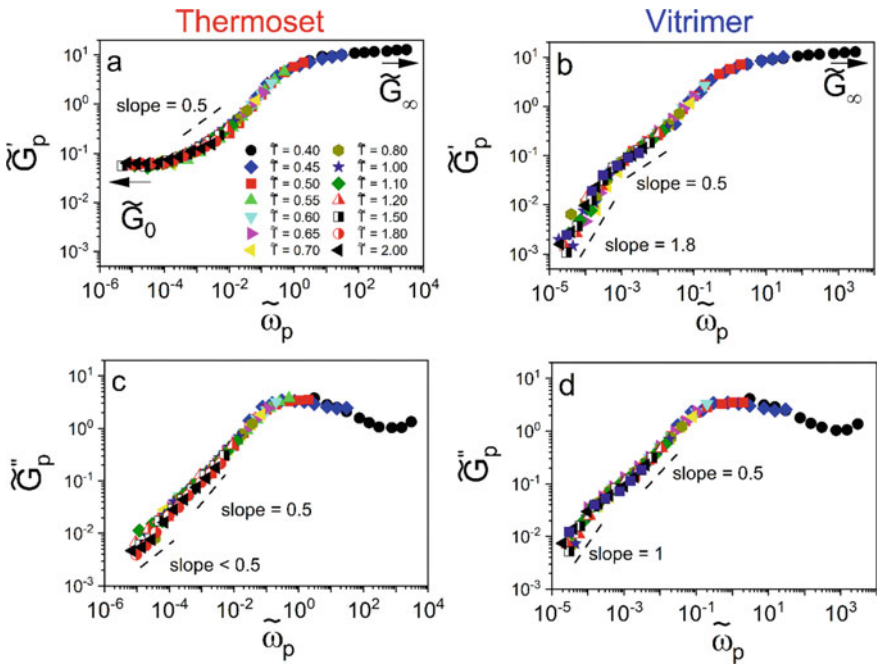

Fig. 7 Universal curves of rescaled **a–b** elastic $\tilde{G}'_p$ and **c–d** loss $\tilde{G}''_p$ moduli as a function of the reduced frequency $\tilde{\omega}_p$ in the model thermoset (left panel) and vitrimer (right panel). The reference temperature in both sets of master curves is $\tilde{T}_0 = 0.6$. The figure is obtained from Perego, Khabaz; Volumetric and Rheological Properties of Vitrimers: A Hybrid Molecular Dynamics and Monte Carlo Simulation Study; Macromolecules; 2020; American Chemical Society

The nonlinear mechanics of vitrimers have also been studied using the hybrid MD–MC method [49] when the exchange reaction rate was adjusted by introducing a constant parameter α in the MC step to adjust the downhill moves energy barrier. The model system was constructed using a tetrafunctional crosslinker and 5-mer monomer chain. The mobility of the vitrimer network showed an inverse relationship with the α value, *i.e.*, smaller values of α led to more frequent bond exchanges in the system, and crosslinker particles could move large distances. Using the NEMD technique, the stress–strain curves of the vitrimer models with different exchange rates under uniaxial deformation were determined at three different temperatures (Fig. 9a–f). Note that the stress–strain curves are plotted until the failure point. When the temperature is below the $\tilde{T}_g$, the thermoset and vitrimer networks with varying values of α show similar behavior at low strain values. On the other hand, when the strain becomes larger, and the response of the networks to the strain becomes nonlinear, vitrimers with slower bond exchanges show a closer stress–strain behavior to the thermoset one. At higher temperatures, we also see the same behavior with a difference that the magnitude of the stress decreases at the failure point. In all cases,

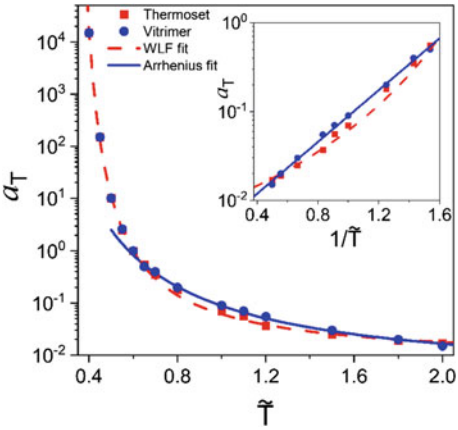

Fig. 8 Horizontal shift factors a_T used in collapsing the moduli data in Fig. 7 for the thermoset and vitrimer as a function of the temperature. Inset: Arrhenius plot of the shift factors obtained at $T > T_v$. The WLF and Arrhenius fit to the data are shown by blue and dashed red lines, respectively. The figure is obtained from Perego, Khabaz; Volumetric and Rheological Properties of Vitrimers: A Hybrid Molecular Dynamics and Monte Carlo Simulation Study; Macromolecules; 2020; American Chemical Society

vitrimers outperform thermoset networks in the failure strain. This strain increases by decreasing the value α.

2.2 Continuum Models

2.2.1 Constitutive Equations

On a continuum level, most of the current models are built on the approach pioneered by Terentjev and coworkers, where they developed a set of microscopic constitutive equations to describe transient polymer networks (such as vitrimers and other self-healing materials) undergoing small deformations in stress relaxation, creep, and uniaxial deformation experiments [71, 72]. In their approach, the energy of the system is described by treating the polymers as Gaussian chains (*i.e.*, Neo-Hookean model) [73]. Here, we briefly review the main features of the constitutive equations, and the reader is referred to ref. [73–75] for detailed derivations.

Breaking and Reforming of Cross-links: Microscopically, the rate of crosslinks breakage can be described using the local force acting on the chain. Assuming a potential energy well with a characteristic energy barrier, in which the crosslink is held, one can derive an equation for a total number of crosslinked chains at a given time $N_c(t)$:

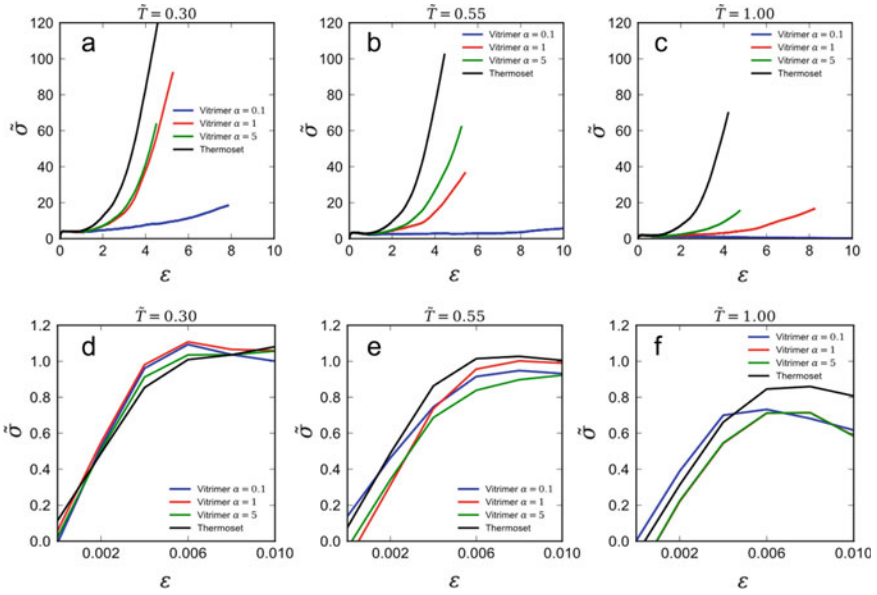

Fig. 9 Stress-strain curves at different temperatures of the simulated thermoset and vitrimer system for various values of α. **d–f** are zoomed-in graphs of **a–c,** respectively, used to show the initial linear response of the four networks. The strain rate used for all the simulations was $\dot{\tilde{\varepsilon}} = 10^{-1}$. The figure is obtained from Perego, Khabaz; Effect of bond exchange rate on dynamics and mechanics of vitrimers; J. Poly. Sci.; 2021; Wiley

$$N_c(t) = N_c(0)\exp\left(-\int_0^t \beta(t';0)dt'\right) + \int_0^t N_b(t')\exp\left(-\int_{t'}^t \beta(t'';t')dt''\right)\rho dt', \tag{4}$$

where β is the equilibrium Kramers rate [74], ρ the effective rate or re-crosslinking, and $N_b(t)$ is the number of un-cross linked chains at a given time. The first term of Eq. (1) indicates the crosslinked chains from $t\prime = 0$ as a function of time. The re-crosslinking of the chains, from the original chains and other chains broken at different times during the same period, is represented by the second term. As $N_b(t) = N_{\text{tot}} - N_c(t)$, Eq. (4) can be seen as an integral equation that helps to determine $N_c(t)$ at a particular dynamic deformation state.

Macroscopic Elastic Energy: The structure of the deformation energy can be characterized macroscopically by adopting Gaussian chains approximation (e.g., using rubber elasticity theory) [75]. For a permanently crosslinked rubbery network, the system's energy density while being deformed is described as:

$$F_{\text{rub}}(t;0) = \frac{1}{2}G\big(\text{tr}\big[\mathbf{E}^{T}(t;0)\mathbf{E}(t;0)\big] - 3\big), \tag{5}$$

where G represents the shear modulus and $\mathbf{E}(t;0)$ is the affine deformation tensor at time t to $t = 0$, which is the reference state.

However, for a transient network undergoing deformation, there are numerous contributions to the average elastic-free energy due to the dynamics of the crosslinks. Thus, the elastic free energy density $F(t;t_0)$ with regards to the reference state t_0 is determined by the deformation tensor $\mathbf{E}(t;t_0)$ defined as:

$$\mathbf{E}(t;t_0) = \mathbf{E}(t;0)\cdot\mathbf{E}^{-1}(t_0;0), \tag{6}$$

The energy density can then be written as:

$$\begin{aligned} F_{\text{tr.}n.}(t) \; &= \exp\left(-\int_0^t \beta(t';0)dt'\right) F_{\text{rub}}(t;0) \\ &+ \int_0^t \rho\frac{N_b(t')}{N_c(0)}\exp\left(-\int_{t\prime}^t \beta\big(t'',t\prime\big)dt''\right) F_{\text{rub}}(t;t\prime)dt', \end{aligned} \tag{7}$$

The second term is computed using the dynamically changing strain tensor defined in Eq. (6) is used to calculate the neo-Hookean free energy density.

Contrary to a permanent rubbery network where the reference state is at $t = 0$, in a transient network, the reference can only be locally specified for different chains, depending on their time of crosslinking. Tracking the real-reference state thus becomes a difficult task, and it is appropriate to describe an effective shear modulus G^* as the following ratio:

$$G^*(t) = \frac{2F_{\text{tr.}n}(t)}{\text{tr}\big[\mathbf{E}^{\text{T}}(t;0)\cdot\mathbf{E}(t_0;0)\big] - 3} \tag{8}$$

Elastic Stress Tensor: In transient networks, the stress is defined by both the elastic and viscous stresses ($\boldsymbol{\sigma}^{\text{ela}}+\boldsymbol{\sigma}^{\text{vis}}$). As the origins of $\boldsymbol{\sigma}^{\text{vis}}$ are very complex (*e.g.,* dangling chains, nonaffine movement of crosslinks and the dynamics of entanglements), it is convenient to express this term as:

$$\boldsymbol{\sigma}^{\text{vis}} = \boldsymbol{\eta}(\dot{\gamma})\cdot\dot{\gamma}, \tag{9}$$

with the viscosity tensor $\boldsymbol{\eta}$ defined as a function of the strain rate tensor $\dot{\gamma}$.

To account for the material incompressibility, it is possible to work with the Gibbs free energy of the system as:

$$g(t) = F_{tr.n.}(t) - p\cdot\det\mathbf{E}. \tag{10}$$

By defining the elastic stress, σ_{ij}^{ela}, as a function of $g(t)$ (*e.g.*, $\sigma_{ij}^{ela}(t) = \frac{\sigma g(t)}{\delta E_{ij}(t;0)}$), the expression for the stress tensor can be obtained:

$$\begin{aligned}\sigma_{ij}^{ela}(t) &= \exp\left(-\int_0^t \beta(t\prime;0)dt\prime\right) G E_{ij}(t;0) \\ &+ \int_0^t \int \rho \frac{N_b(t\prime)}{N_c(0)} \exp\left(-\int_{t\prime}^t \beta(t\prime\prime,t\prime)dt\prime\prime\right) G E_{jk}(t;t\prime) E_{jk}^{-1}(t\prime;0)dt\prime \\ &- p \cdot \det \mathbf{E} \cdot E_{ji}^{-1}. \end{aligned} \tag{11}$$

Equation (11) provides the constitutive equation of the model and can be used to study how a transient network responds to an imposed uniaxial stretch. Figure 10a shows a schematic of a polymer sheet undergoing uniaxial stretching**.** By defining the length (L), width (W), and thickness (T) elongation ratios as λ_L, λ_W, and λ_T, respectively, the deformation can be described using the following relationships: $L = \lambda_L L_0$, $W = \lambda_W W_0$, and $T = \lambda_T H_T$. Due to the incompressibility of the system, one can write $\lambda_L = \lambda$ making λ_W together with λ_T equal to $1/\sqrt{\lambda}$.

The deformation tensor at a time t for a particular crosslink formed a time $t\prime$ can be obtained through Eq. (6):

$$\mathbf{E}(t;t\prime) = \frac{\lambda(t)}{\lambda(t\prime)} \mathbf{e}_L \mathbf{e}_L + \sqrt{\frac{\lambda(t\prime)}{\lambda(t)}} (\mathbf{e}_W \mathbf{e}_W + \mathbf{e}_T \mathbf{e}_T), \tag{12}$$

with $\mathbf{e}_L$, $\mathbf{e}_W$, and $\mathbf{e}_T$ as the unit vectors in three orthogonal directions. The average end-to-end distance $\langle r \rangle$ (Fig. 9b) that indicates the deformation occurring at a time t with respect to a reference time τ can then be calculated using:

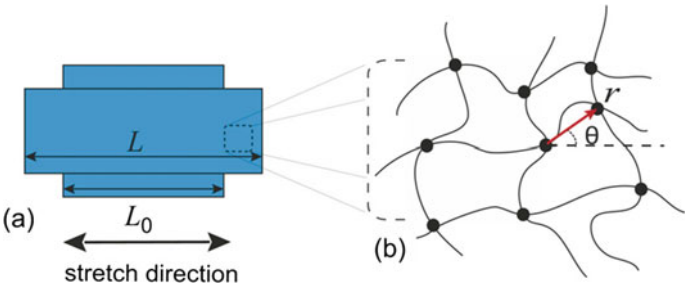

Fig. 10 **a** Illustration of a polymeric sheet undergoing uniaxial stretched deformation. **b** schematic of a sample of polymer chains in the network undergoing the same deformation, with r as the end-to-end distance and θ as the angle between the end-to-end vector and the stretch direction. The figure is obtained from Meng, Pritchard, Terentjev; Stress Relaxation, Dynamics, and Plasticity of Transient Polymer Networks; Macromolecules; 2016; American Chemical Society

$$\langle r_{t;\tau} \rangle = r_0 \int_0^{\pi/2} d\theta \sin\theta \sqrt{\left(\frac{\lambda(t)}{\lambda(\tau)}\right)^2 \cos^2\theta + \left(\frac{\lambda(\tau)}{\lambda(t)}\right)^2 \sin^2\theta}, \tag{13}$$

with $r_0 \sim \sqrt{N_s} b$ being the network mesh size in its reference state. The transient network's elastic free energy can be expressed as:

$$\begin{aligned} F_{\text{tr.n.}}(t) &= \exp\left(-\int_0^t \beta(t';0)dt'\right) F_{\text{rub}}(t;0) \\ &+ \int_0^t \rho \frac{N_b(t')}{N_c(0)} \exp\left(-\int_{t'}^t \beta(t'',t')dt''\right) F_{\text{rub}}(t;t')dt'. \end{aligned} \tag{14}$$

Similarly, using Eq. (8) and dividing both the terms of Eq. (14) by the characteristic new-Hookean strain, we can obtain the effective shear modulus:

$$\begin{aligned} G^*(t) &= G \exp\left(-\int_0^t \beta(t';0)dt'\right) \\ &+ G \int_0^t \rho \frac{N_b(t')}{N_0} \exp\left(-\int_{t'}^t \beta(t'';t')dt''\right) \\ &\times \left(\frac{\lambda(t)^2/\lambda(t\prime)^2 + 2\lambda(t')/\lambda(t) - 3}{\lambda(t)^2 + 2/\lambda(t) - 3}\right) dt'. \end{aligned} \tag{15}$$

Using Eq. (11)**,** it is possible to calculate the transverse diagonal components of the stress, thus obtaining:

$$\begin{aligned} \sigma_L(\lambda,t) &= G \exp\left(-\int_0^t \beta(t\prime;0)dt\prime\right)\left(\lambda(t) - \frac{1}{\lambda(t)^2}\right) \\ &+ G \int_0^t \frac{N_b(t\prime)}{N_0} \rho \exp\left(-\int_{t'}^t \beta(t\prime\prime;t\prime)dt\prime\prime\right)\left(\frac{\lambda(t)}{\lambda(t\prime)^2} - \frac{\lambda(t\prime)}{\lambda(t)^2}\right) dt\prime. \end{aligned} \tag{16}$$

Thus, to calculate this dynamic stress under uniaxial deformation, one must first solve Eq. (4) to determine $N_b(t)$ and subsequently compute the time-integrals of Eq. (16).

Stress-relaxation: The simplest way to test model accuracy is to compute the stress relaxation behavior of the transient network when a uniaxial stepwise deformation λ is applied at $t = 0$. In this scenario, $\lambda(t) = \lambda(t\prime)$ makes the second term of Eq. (15) equal to zero. The tensile stress can be easily computed along the stretching direction

from Eq. (16), thus obtaining:

$$\sigma_L = Ge^{\beta(\lambda)t}\left(\lambda - \frac{1}{\lambda^2}\right). \tag{17}$$

Equation (17) shows how the stress relaxes following a stretched exponential form with the characteristic relaxation time defined as $\tau = 1/\beta(\lambda)$ [76, 77]. Using Eq. (13) to calculate the average end-to-end chain length, we can write the explicit form of $\beta(\lambda)$ as:

$$\begin{aligned}\beta(\lambda) &= \omega_0 \exp\left(\kappa r_o \int_0^{\pi/2} \sin\theta\sqrt{(1/\lambda)}\sin\right) \exp(-W_b/k_bT) \\ &= c_0(\lambda)\exp(-W_b/k_bT),\end{aligned} \tag{18}$$

with

$$c_0(\lambda) = \omega_0 \exp\left[\frac{3}{2\sqrt{N_s}\lambda}\left(\lambda^{3/2} + \frac{\operatorname{arcsinh}\left(\sqrt{\left(\lambda^3-1\right)}\right)}{\sqrt{\left(\lambda^3-1\right)}}\right)\right] \tag{19}$$

Equation (19) indicates that $c_0(\lambda)$ increases monotonically with the stretching ratio λ. At lower limits (small strain) $c_0 \approx \omega_0 \exp\left(3/\sqrt{(N_s)}\right)$ while at upper limit (high strain) $c_0 \approx \omega_0 \exp\left(3\lambda/2\sqrt{(N_s)}\right)$. The theoretical normalized shear modulus $G(t)/G_{max}$ (Fig. 11)of two vitrimer systems shows an excellent agreement with the experimental data obtained by Montarnal et al. [5] and rom Hillmyer et al. [33].

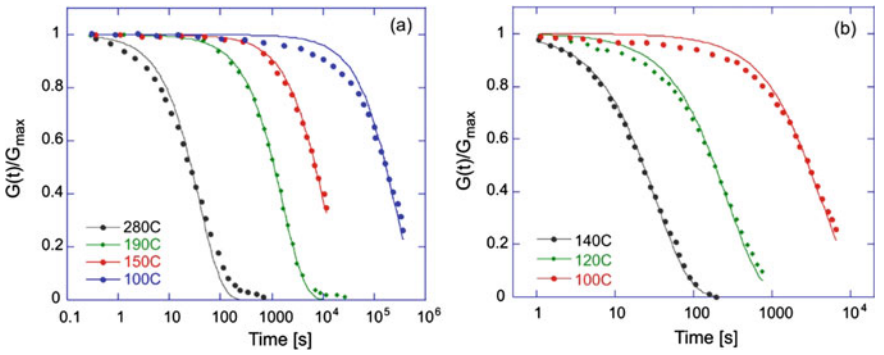

Fig. 11 Normalized shear modulus $G(t)/G_{max}$ as a function of relaxation time at different temperatures. The solid lines are the predicted values from the model, and the markers are the experimental data from **a** Montarnal et al. [5] (epoxy vitrimer) and **b** from Hillmyer et al. [33] (polylactide vitrimer). The figure is obtained from Meng, Pritchard, Terentjev; Stress Relaxation, Dynamics, and Plasticity of Transient Polymer Networks; Macromolecules; 2016; American Chemical Society

The takeaway message is that stress relaxation in transient networks decays in a stretched exponential manner. In contrast to ordinary rubbers which relax under stress, this behavior, due to the permanent nature of the crosslinks, displays a long-time power-law/logarithmic tail.

The authors further demonstrate the accuracy of the proposed model by performing a strain-ramp simulation on the system. The results show remarkable agreement with the experimental values obtained for various vitrimer systems. The proposed theoretical framework highlighted that the material response is strongly influenced by the crosslinker exchange kinetics. However, the model was built using several approximations. For example, the nonaffine displacement of the system is not considered in the development of the theory. This is particularly crucial when the entangled chain mobility is significant. Additionally, the neo-Hookean model is only valid for deformation below 100% strain. When dealing with larger deformations, different elastic models should be implemented. Despite these limitations, the proposed model provided an excellent picture of the dynamics and relaxation in vitrimers and laid the foundation for developing subsequent continuum models for transient networks.

2.2.2 FEA Implementation

Continuing within the scope of continuum mechanics, Qi and coworkers developed a model which successfully accounts for the coupling between the macroscopic and microscopic properties of the network (*e.g.* bond exchange reactions) [77]. Their basic approach was built based on the idea developed by Tobolsky et al. [77, 79] in which, during the loading history, the polymer network is broken down into two groups of chains, each one reforming at a different period.

The model requires the following fields variables to be solved for: temperature T, the chain composition as a function of time $C_{OR}(t)$ and $\Delta(\tau, t)$, the Lagrangian multiplier p (used to reinforce isothermal incompressibility), as well as the displacement vector $\mathbf{u} \equiv \mathbf{x} - \mathbf{X}$ which describes the deformed position. These five coupled equations that connect these five variables are as follows:

1. Energy balance:

$$\left[\gamma + \frac{\mathrm{S{:}F}}{3}\left(\alpha_{\mathrm{v}} + \frac{\mathrm{d}\alpha_{\mathrm{v}}}{\mathrm{d}T}T\right)\right]\dot{\mathrm{T}} = \left(1 - \frac{\alpha_{\mathrm{v}}\mathrm{T}}{3}\right)\mathrm{S}{:}\,\dot{\mathrm{F}} - \nabla_{\mathrm{x}} \cdot \mathrm{Q} + \Psi - \frac{\alpha_{\mathrm{v}}\mathrm{T}}{3}\,\dot{\mathrm{S}}\,{:}\mathrm{F}, \tag{20}$$

where γ is the specific heat per unit volume, S is the first Piola–Kirchhoff (nominal), stress tensor, F is the deformation gradient, α_v is the thermal expansion coefficient, T is the temperature, Q is the heat flux vector, and Ψ is the rate of eternal heat supply per unit volume. The dot on top of the variables denotes the material time derivative. The x in the subscript of the gradient operator denoted the gradient being taken with respect to the reference configuration.

2. Linear momentum balance

$$\nabla_x \cdot \mathrm{S}^{\mathrm{T}} + \mathrm{b} = 0, \tag{21}$$

where b is the body force vector per unit volume.

3. Incompressibility constraint

$$\det(\boldsymbol{F}_t) = J_t = \left(F_{\mathrm{t}}^a\right)^3 = \exp\left(\int_{T_0}^{T} \alpha_v\left(\tilde{T}\right) d\tilde{T}\right), \tag{22}$$

where F_t^a is the thermal component of F at the deformation time t.

4. Constitutive equation for the normal stress tensor

$$\begin{aligned} \mathrm{S} \; &= -\frac{p}{F_t^a}\left(\mathrm{F}_t^e\right)^{-T} \\ &+ \frac{C_{\mathrm{OR}}}{F_t^a C_0}\Omega(I(t))\mathrm{F}_t^e \\ &+ \int_0^t \left[\frac{\Delta(\tau,t)}{F_t^a C_0}\Omega(H(\tau,t))\mathrm{F}_t^e\left(\mathrm{F}_\tau^e\right)^{-1}\left(\mathrm{F}_\tau^e\right)^{-T}\right] d\tau, \end{aligned} \tag{23}$$

where:

$$\Omega(y) \equiv \frac{C_0 RT\sqrt{N}}{\sqrt{3y}} L^{-1}\left(\sqrt{\frac{y}{3N}}\right), \tag{24}$$

and

$$I(t) \equiv tr\left(\mathrm{F}_t^e\left(\mathrm{F}_t^e\right)^T\right), \;\; H(t,\tau) \equiv tr\left(\mathrm{F}_t^e\left(\mathrm{F}_t^e\right)^{-1}\left(\mathrm{F}_t^e\left(\mathrm{F}_\tau^e\right)^{-1}\right)^T\right), \tag{25}$$

Here, F_t^e is the mechanical component of F at the deformation time t; C_0 is the original (before deformation) molar density of all the polymer chains; N is a material parameter that indicates the length of the chain between crosslinkers. L^{-1} is the inverse Langevin function.

5. Kinetic equations for heat flux and exchange reaction rate

$$\mathrm{Q} = -K_t \det(\mathrm{F})(\mathrm{F}^T\mathrm{F})^{-1}\nabla_x T, \tag{25}$$

$$rdtd\mathrm{v} = -\dot{C}_{\mathrm{OR}} dtdV \Rightarrow \dot{C}_{\mathrm{OR}} = -Jr = -k\exp\left(-\frac{E_a}{RT}\right)C_{\mathrm{OR}}, \tag{26}$$

$$\frac{\partial \Delta(\tau,t)}{\partial t} = -k\exp\left(-\frac{E_a}{RT}\right)\Delta(\tau,t),\ (\tau \le t). \tag{27}$$

Here, K_t is the thermal conductivity; k is a kinetic coefficient (always positive), and E_a is the activation energy of the bond exchange reaction. Initials and boundaries conditions (B.C.) are also necessary to solve these field equations.

The model includes six materials parameters: γ (specific heat), K_b (thermal conductivity), C_0 (original chain density), N (Arruda-Boyce chain segment number), E_a (activation energy), and k (bond exchange rate coefficient). Considering isothermal conditions, one can disregard the thermal parameters γ and K_t from the model, while all other parameters are accessible through stress-relaxation experiments.

To validate the model, it is important to consider the case of the uniaxial extension during an isothermal process. Due to isothermal conditions and using the initial B.C., Eq. (26) can be solved for the evolution of the chain composition, to obtain:

$$C_{\mathrm{OR}} = C_0\exp\left(-k\exp\left(-\frac{E_a}{RT}\right)t\right), \tag{28}$$

Likewise, Eq. (29) is solved to yield:

$$\Delta(\tau,t) = k\exp\left(-\frac{E_a}{RT}\right)C_0\exp\left(-k\exp\left(-\frac{E_a}{RT}\right)(t-\tau)\right),\ (\tau \le t). \tag{29}$$

The associative nature of the bond exchange in transient networks enables the total chain density of the system to be calculated by adding the original with the reformed chains together (at any time t the total chain density is equal to C_0). Additionally, by considering isothermal conditions $F^a = 1 \rightarrow \mathbf{F}^e = \mathbf{F}$. The unit vector $\mathbf{e}_1$ denotes the direction of stretching for the sample. λ, $\lambda^{1/2}$, and $\lambda^{1/2}$ are the three principal stresses. To obtain S_{11} (tensile stress along $\mathbf{e}_1$), it is useful to introduce first the following notation:

$$\lambda_t \equiv \lambda(t) \text{ and } \lambda_\tau \equiv \lambda(\tau). \tag{30}$$

We can then write Eq. (25) as:

$$I(t) = \lambda_t^2 + 2/\lambda_t,\ \text{and}\ H(\tau,t) = (\lambda_t/\lambda_\tau)^2 + 2\lambda_\tau/\lambda_t. \tag{31}$$

Finally, substituting Eq. (30) and Eq. (31) into Eq. (23), we obtain:

$$S_{11}(t) = \frac{C_{OR}(t)}{C_0}\Omega(I(t))\left(\lambda_t - \frac{1}{\lambda_t^2}\right) + \int_0^t \left[\frac{\Delta(\tau,t)}{C_0}\Omega(H(\tau,t))\left(\frac{\lambda_t}{\lambda_\tau^2} - \frac{\lambda_\tau}{\lambda_t^2}\right)\right]d\tau. \tag{32}$$

S_{11} represents the applied tensile force per unit cross-sectional area A_0 of the undeformed stress (nominal tensile stress), and it can be used to study the material response for various deformation cases (such as stress relaxation, tensile tests, and creep).

Stress Relaxation

During a stress relaxation experiment, at $t = 0^+$, a constant stretch ratio λ_C is applied. Therefore, $\lambda_t = \lambda_\tau = \lambda_C$ transforming the tensile stress S_{11} in:

$$S_{11}(t) = \left(\lambda_C - \lambda_C^{-2}\right)\Omega\left(\lambda_C^2 + 2/\lambda_C\right)\exp\left(-k\exp\left(-\frac{E_a}{RT}\right)t\right) \tag{33}$$

As seen in the theory developed by Meng et al. [71], the stress decays exponentially with time (e.g., $\frac{S_{11}(t)}{S_{11}(t=0^+)} = \exp\left(-\frac{t}{t_r}\right)$) where $t_R = \frac{1}{k}\exp\left(\frac{E_a}{RT}\right)$ is the characteristic relaxation time. Equation (33) it is also consistent with the observations of Leibler and coworkers, where they illustrate how the kinetics of bond exchange reaction influences t_R [78].

Figure 12a shows the agreement between the tensile stress values calculated by solving Eq. (33) and the experimental data obtained using an epoxy-acid vitrimer network catalyzed with 5 mol% zinc acetate [5]. Solving for the relaxation time t_R and plotting as a function of inverse temperature (Fig. 12b) allows calculating the activation energy of the system. The model predicts a value of $E_a = 81.1$ kJ mol^{-1} which is in agreement with the value of 80 kJ mol^{-1} reported in Montarnal et al. [5].

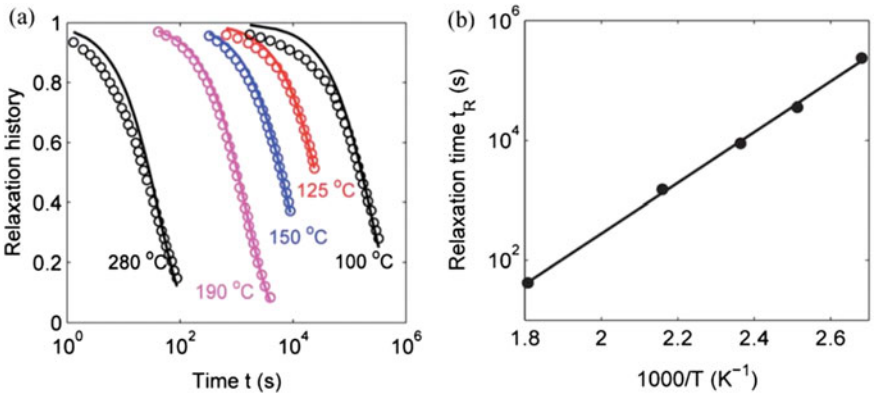

Fig. 12 **a** Stress relaxation curves at different temperatures. The solid lines are the values predicted by the model, while the symbols are the experimental data extracted from Montarnal et al. [5] **b** Relaxation time t_R as a function of inverse temperature. The solid line is the fit according to the model, and the symbols are the values obtained from the fitting of the experimental data [5]. The figure is obtained from Long, Qi, Dunn; Modeling the mechanics of covalently adaptable polymer networks with temperature-dependent bond exchange reactions; Soft Matter; 2013; Royal Society of Chemistry

FEM implementation–Modeling thermoforming processes: The notable feature of this model is that it can be implemented into three-dimensional finite element code (*e.g.,* ABAQUS [80]) using a user material subroutine (UMAT). One of the technologically remarkable properties of vitrimers is their ability to be easily reshaped through thermoforming processes. Thus, the capability to model these types of deformation events is essential from a processing perspective. The following three steps are typical in the thermoforming process:

1. The material undergoes a prescribed deformation at a low temperature (*e.g.*, 25°C).
2. The prescribed deformation is maintained, while the sample is heated over a time period. During this step, the network topology of vitrimers is re-arranged because of the activation of the bond exchange reactions.
3. The sample is cooled, and the applied deformation is released. As the vitrimer undergoes stress relaxation during Step 2, the original shape of the sample will not recover.

Twisting a strip: This simulation is inspired by the experiment used by Montarnal et al. [5] to illustrate the stress relaxation event in vitrimers. A twist angle of 5π is applied to a sample with dimensions $12 \times 1 \times 0.1$ cm. Figure 13 shows results obtained at $T = 523$ K using two processing times ($t_a = 10$ and $t_a = 100$ s). During the stress relaxation (Step 2), the extent of stress relaxation depends substantially on t_a consequently affecting the final shape of the material. At $t_a = 10$ s, as only a modest amount of stress is relaxed, the sample virtually returns to its original shape. In contrast, at $t_a = 100$ s, more stress is relaxed producing the shape memory in the material. These observations are also consistent with the experiments of Montarnal et al. [5] Generally, upon increasing temperature, less processing time is necessary to increase the rate of stress relaxation. To explore this effect more quantitatively, a fixity parameter can be introduced as the ratio of the deformation obtained after thermoforming and the given initially prescribed deformation (for more details, see Long et al. [42]).

Although this model shows remarkable agreement with stress-relaxation experiments, it still lacks the ability to capture some important features observed in vitrimers. For example, the model shows a shortcoming to describe the network's hysteresis accurately and creep compliance behavior. Furthermore, this continuum model does not account for heat conduction and thermal expansions events observed during thermo-mechanical tests. This is particularly crucial if local heat is used to process the material [77].

To account for some of the shortcomings of the model presented by Qi and coworkers, such as the inability to study surface welding on the material, a more robust multiscale modeling framework was developed in 2016 by Yu et al. [81]. In this theoretical model, the dependency of interfacial kinetics of vitrimers was studied under various mechanical and thermal fields. Their approach was firstly to model the kinetics of the bond exchange reaction at the macromolecular scale. This model was used to capture the effect of bond exchange on the evolution of the chain density at the interface.

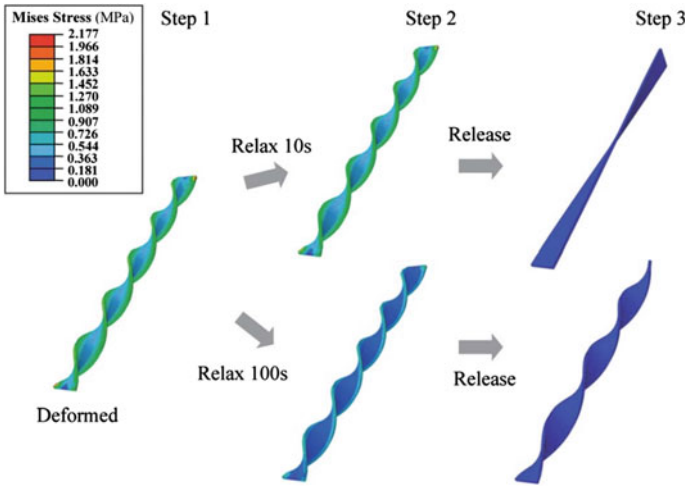

Fig. 13 FEM simulation of the thermoforming process in vitrimer network. The temperature used is 523 K. Two processing times are shown: 10 and 100 s. The figure is obtained from Long, Qi, Dunn; Modeling the mechanics of covalently adaptable polymer networks with temperature-dependent bond exchange reactions; Soft Matter; 2013; Royal Society of Chemistry

In later studies, a cohesive zone approach was incorporated with the model to predict the behavior of epoxy vitrimers undergoing interfacial welding and failure. Using this multiscale model, the chain density and fracture energy of the material can be obtained and later be used as input parameters for the FEM simulations. The proposed multiscale model can also be used to analyze more complex welding problems like polymer reprocessing with irregular shape and particle size [82].

2.2.3 Outlook

Although the mentioned models successfully account for the kinetics of the bonds exchange reactions of vitrimers, they all still rely on elastic models on the continuum level such as neo-Hookean and Arruda–Boyce. Consequently, they cannot provide a direct comparison between the macroscopic mechanics of the network and the single-chain physics of the polymer. As a result, using those models to describe more complex molecular phenomena like entanglement and chain diffusion becomes fundamentally challenging. In addition, both models require a large number of materials parameters and variables to be successfully implemented computationally. To address these limitations, Vernerey et al. [83] introduced a statistically based continuum theory for transient networks polymers. In their framework, the polymer physical state is characterized by a statistical distribution of the length and direction of the end-to-end chains. Both macroscopic deformations and molecular-level events can be used to alter this distribution. Using a so-called distribution tensor, it is possible to relate the chain distribution to stress, strain, and entropy of the network.

This model provides an extension of the classic rubber elasticity theory. It is usable in the range of inelastic deformation, and it can be extended to account for large-chain deformations.

3 Conclusions

Vitrimers provide a practical route for synthesizing intrinsic self-healing materials and reprocessing thermosets. Particle-based simulations techniques mainly utilize patchy particles [50], three-body potential [80], and hybrid MD–MC methods to describe the bond swap between the crosslinkers. The patchy particles model successfully predicts the Arrhenius-like behavior zero shear viscosity of vitrimers that has been observed in experiments. Using the three-body potential for bond swapping, it was shown that the stress relaxation modulus of transient networks exhibits a secondary relaxation due to the change in the network topology [46]. Recently [48], we employed a hybrid MD–MC technique to simulate and predict the dynamics of a model vitrimer and evaluate its thermodynamics and rheological properties. Our simulations showed that the topology freezing temperature, which marks the transition from the rubbery to the viscoelastic fluid regime in vitrimers, can be detected from volumetric and rheological data. The onset of the network rearrangement was related to the lifetime of the exchangeable bonds, which determines the rheology of the network. The current simulation frameworks [48, 49, 56, 80] provide an excellent opportunity to study the linear and nonlinear rheology and mechanics of vitrimers with different topologies. One can adjust the bond exchange rate and control the competition between self-healing ability in the rubber and the damage caused by external stimuli and design the final rubber product with superior mechanical strength, re-processability, and self-healing property.

On a continuum level, different network models have been developed to study transient polymer networks such as vitrimers undergoing small to large deformations. By treating the polymer chains as neo-Hookian chains and starting from the classic theory of rubber elasticity, it is possible to derive constitutive equations that accurately predict the stress relaxation behavior of these networks [71]. Consistent with experimental observations [5], these models show that stress relaxation in vitrimers decays in a stretched exponential manner contrary to the long-time power-law/logarithmic tail observed in permanently crosslinked networks [4]. Additionally, energy balances can be incorporated to account for the coupling between the macroscopic thermo-mechanics and microscopic bond exchange reactions of vitrimers [77]. Continuum models can also be implemented in commercially available FEA software to simulate processes such as thermoforming and polymer welding [77].

Considering the current developments in the field of vitrimers, it is of interest to investigate the rheology and mechanics of vitrimers as a function of network topology, the energy barrier of the bond exchange and chemistry of the network, and identify the underlying mechanism of macroscopic flow behavior, fracture,

and fatigue at different service conditions in these networks, which combines recyclability and self-healing ability with maximum solvent resistance.

References

1. Blaiszik, B.J., Kramer, S.L., Olugebefola, S.C., Moore, J.S., Sottos, N.R., White, S.R.: Self-healing polymers and composites. Annu. Rev. Mater. Res. **40**, 179–211 (2010)
2. Wool, R.P.: Self-healing materials: a review. Soft Matter **4**(3), 400–418 (2008)
3. Ghosh, S.K.: Self-healing materials: fundamentals, design strategies, and applications. Wiley Online Library (2009)
4. Cordier, P., Tournilhac, F., Soulié-Ziakovic, C., Leibler, L.: Self-healing and thermoreversible rubber from supramolecular assembly. Nat. **451**(7181), 977–980 (2008)
5. Montarnal, D., Capelot, M., Tournilhac, F., Leibler, L.: Silica-like malleable materials from permanent organic networks. Sci. **334**(6058), 965–968 (2011)
6. Röttger, M., Domenech, T., van der Weegen, R., Breuillac, A., Nicolaÿ, R., Leibler, L.: High-performance vitrimers from commodity thermoplastics through dioxaborolane metathesis. Sci. **356**(6333), 62–65 (2017). https://doi.org/10.1126/science.aah5281
7. Poliskie, M.: Solar module packaging: polymeric requirements and selection. CRC Press(2016)
8. Rubinstein, M., Colby, R.H.: Polymer physics, vol. 23. Oxford University Press, New York (2003)
9. Tabor, D., Tabor, D.: Gases, liquids and solids: and other states of matter. Cambridge University Press (1991)
10. Ferry, J.D.: Viscoelastic properties of polymers. Wiley (1980)
11. Angell, C.A.: Formation of glasses from liquids and biopolymers. Sci. **267**(5206), 1924–1935 (1995). https://doi.org/10.1126/science.267.5206.1924
12. Biron, M.: Thermoplastics and thermoplastic composites. William Andrew (2018)
13. Van Zee, N.J., Nicolaÿ, R.: Vitrimers: permanently crosslinked polymers with dynamic network topology. Prog. Polym. Sci. 101233 (2020)
14. Dodiuk, H., Goodman, S.H.: Handbook of thermoset plastics. William Andrew (2013)
15. Kutz, M.: Applied plastics engineering handbook: processing, materials, and applications. William Andrew(2016)
16. Ibarra, R.M.: Recycling of thermosets and their composites. In: Thermosets, pp. 639–666. Elsevier (2018)
17. Pickering, S.J.: Recycling technologies for thermoset composite materials—current status. Compos. A **37**(8), 1206–1215 (2006)
18. Geyer, R., Jambeck, J.R., Law, K.L.: Production, use, and fate of all plastics ever made. Sci. Adv. **3**(7), e1700782 (2017)
19. Bowman, C.N., Kloxin, C.J.: Covalent adaptable networks: reversible bond structures incorporated in polymer networks. Angew. Chem. Int. Ed. **51**(18), 4272–4274 (2012)
20. Herbst, F., Döhler, D., Michael, P., Binder, W.H.: Self-healing polymers via supramolecular forces. Macromol. Rapid Commun. **34**(3), 203–220 (2013)
21. Thakur, V.K., Kessler, M.R.: Self-healing polymer nanocomposite materials: a review. Polym. **69**, 369–383 (2015)
22. Higaki, Y., Otsuka, H., Takahara, A.: A thermodynamic polymer crosslinking system based on radically exchangeable covalent bonds. Macromolecules **39**(6), 2121–2125 (2006)
23. Drozdov, A., Christiansen, Jd.: Thermo-mechanical behavior of elastomers with dynamic covalent bonds. Int. J. Eng. Sci. 147, 103200 (2020)
24. Krishnakumar, B., Sanka, R.P., Binder, W.H., Parthasarthy, V., Rana, S., Karak, N.: Vitrimers: associative dynamic covalent adaptive networks in thermoset polymers. Chem. Eng. J. **385**, 123820 (2020)

25. Denissen, W., Winne, J.M., Du Prez, F.E.: Vitrimers: permanent organic networks with glass-like fluidity. Chem. Sci. **7**(1), 30–38 (2016)
26. Capelot, M., Montarnal, D., Tournilhac, F., Leibler, L.: Metal-catalyzed transesterification for healing and assembling of thermosets. J. Am. Chem. Soc. **134**(18), 7664–7667 (2012). https://doi.org/10.1021/ja302894k
27. Denissen, W., Rivero, G., Nicolaÿ, R., Leibler, L., Winne, J.M., Du Prez, F.E.: Vinylogous urethane vitrimers. Adv. Funct. Mater. **25**(16), 2451–2457 (2015)
28. Winne, J.M., Leibler, L., Du Prez, F.E.: Dynamic covalent chemistry in polymer networks: a mechanistic perspective. Polym. Chem. **10**(45), 6091–6108 (2019)
29. Scott, T.F., Schneider, A.D., Cook, W.D., Bowman, C.N.: Photoinduced plasticity in crosslinked polymers. Sci. **308**(5728), 1615–1617 (2005)
30. Amamoto, Y., Kamada, J., Otsuka, H., Takahara, A., Matyjaszewski, K.: Repeatable photoinduced self-healing of covalently crosslinked polymers through reshuffling of trithiocarbonate units. Angew. Chem. Int. Ed. **50**(7), 1660–1663 (2011)
31. Dahlke, J., Zechel, S., Hager, M.D., Schubert, U.S.: How to design a self-healing polymer: general concepts of dynamic covalent bonds and their application for intrinsic healable materials. Adv. Mater. Interfaces **5**(17), 1800051 (2018)
32. Montarnal, D., Tournilhac, F., Hidalgo, M., Leibler, L.: Epoxy-based networks combining chemical and supramolecular hydrogen-bonding crosslinks. J. Polym. Sci. Part A Polym. Chem. **48**(5), 1133–1141 (2010)
33. Brutman, J.P., Delgado, P.A., Hillmyer, M.A.: Polylactide vitrimers. ACS Macro Lett. **3**(7), 607–610 (2014)
34. Fortman, D.J., Brutman, J.P., Cramer, C.J., Hillmyer, M.A., Dichtel, W.R.: Mechanically activated, catalyst-free polyhydroxyurethane vitrimers. J. Am. Chem. Soc. **137**(44), 14019–14022 (2015). https://doi.org/10.1021/jacs.5b08084
35. Yang, Y., Pei, Z., Li, Z., Wei, Y., Ji, Y.: Making and remaking dynamic 3D structures by shining light on flat liquid crystalline vitrimer films without a mold. J. Am. Chem. Soc. **138**(7), 2118–2121 (2016). https://doi.org/10.1021/jacs.5b12531
36. Pei, Z., Yang, Y., Chen, Q., Wei, Y., Ji, Y.: Regional Shape Control of Strategically Assembled Multishape Memory Vitrimers. Adv. Mater. **28**(1), 156–160 (2016). https://doi.org/10.1002/adma.201503789
37. Zheng, N., Fang, Z., Zou, W., Zhao, Q., Xie, T.: Thermoset shape-memory polyurethane with intrinsic plasticity enabled by transcarbamoylation. Angew. Chem. Int. Ed. **55**(38), 11421–11425 (2016)
38. Capelot, M., Unterlass, M.M., Tournilhac, F., Leibler, L.: Catalytic control of the vitrimer glass transition. ACS Macro Lett. **1**(7), 789–792 (2012)
39. Ricarte, R.G., Tournilhac, F., Cloître, M., Leibler, L.: Linear viscoelasticity and flow of self-assembled vitrimers: the case of a polyethylene/dioxaborolane system. Macromolecules **53**(5), 1852–1866 (2020)
40. Smallenburg, F., Leibler, L., Sciortino, F.: Patchy particle model for vitrimers. Phys. Rev. Lett. **111**(18), 188002 (2013)
41. Dyre, J.C.: Colloquium: the glass transition and elastic models of glass-forming liquids. Rev. Mod. Phys. **78**(3), 953–972 (2006). https://doi.org/10.1103/RevModPhys.78.953
42. Long, R., Qi, H.J., Dunn, M.L.: Modeling the mechanics of covalently adaptable polymer networks with temperature-dependent bond exchange reactions. Soft Matter **9**(15), 4083–4096 (2013)
43. Ciarella, S., Ellenbroek, W.G.: Swap-driven self-adhesion and healing of vitrimers. Coat. **9**(2), 114 (2019)
44. Ciarella, S., Biezemans, R.A., Janssen, L.M.: Understanding, predicting, and tuning the fragility of vitrimeric polymers. Proc. Natl. Acad. Sci. **116**(50), 25013–25022 (2019)
45. Wertheim, M.: Thermodynamic perturbation theory of polymerization. J. Chem. Phys. **87**(12), 7323–7331 (1987)
46. Rovigatti, L., Nava, G., Bellini, T., Sciortino, F.: Self-dynamics and collective swap-driven dynamics in a particle model for vitrimers. Macromolecules **51**(3), 1232–1241 (2018)

47. Singh, K., Rabin, Y.: Aging of thermoreversible gel of associating polymers. Macromolecules **53**(10), 3883–3890 (2020). https://doi.org/10.1021/acs.macromol.0c00258
48. Perego, A., Khabaz, F.: Volumetric and rheological properties of vitrimers: a hybrid molecular dynamics and Monte Carlo simulation study. Macromolecules **53**(19), 8406–8416 (2020). https://doi.org/10.1021/acs.macromol.0c01423
49. Perego, A., Khabaz, F.: Effect of bond exchange rate on dynamics and mechanics of vitrimers. J. Polym. Sci. **59**(21), 2590–2602 (2021)
50. Smallenburg, F., Leibler, L., Sciortino, F.: Patchy particle model for vitrimers. Phys. Rev. Lett. **111**, 1–5 (2013). https://doi.org/10.1103/PhysRevLett.111.188002
51. Wertheim, M.: Fluids with highly directional attractive forces. I. Statistical thermodynamics. J. Stat. Phys. **35**(1), 19–34 (1984)
52. Kern, N., Frenkel, D.: Fluid–fluid coexistence in colloidal systems with short-ranged strongly directional attraction. J. Chem. Phys. **118**(21), 9882–9889 (2003)
53. Kremer, K., Grest, G.S.: Dynamics of entangled linear polymer melts: A molecular-dynamics simulation. J. Chem. Phys. **92**(8), 5057–5086 (1990)
54. Weeks, J.D., Chandler, D., Andersen, H.C.: Role of repulsive forces in determining the equilibrium structure of simple liquids. J. Chem. Phys. **54**(12), 5237–5247 (1971)
55. Stillinger, F.H., Weber, T.A.: Computer simulation of local order in condensed phases of silicon. Phys. Rev. B **31**(8), 5262 (1985)
56. Ciarella, S., Sciortino, F., Ellenbroek, W.G.: Dynamics of vitrimers: defects as a highway to stress relaxation. Phys. Rev. Lett. **121**(5) (2018). https://doi.org/10.1103/physrevlett.121.058003
57. Kubo, R.: Statistical-mechanical theory of irreversible processes. I. General theory and simple applications to magnetic and conduction problems. J. Phys. Soc. Jpn. **12**(6), 570–586 (1957)
58. Pant, P.K., Theodorou, D.N.: Variable connectivity method for the atomistic Monte Carlo simulation of polydisperse polymer melts. Macromolecules **28**(21), 7224–7234 (1995)
59. Karayiannis, N.C., Mavrantzas, V.G., Theodorou, D.N.: A novel Monte Carlo scheme for the rapid equilibration of atomistic model polymer systems of precisely defined molecular architecture. Phys. Rev. Lett. **88**(10), 105503 (2002)
60. Sides, S.W., Grest, G.S., Stevens, M.J., Plimpton, S.J.: Effect of end-tethered polymers on surface adhesion of glassy polymers. J. Polym. Sci. Part B Polym. Phys. **42**(2), 199–208 (2004)
61. Hoy, R.S., Fredrickson, G.H.: Thermoreversible associating polymer networks. I. Interplay of thermodynamics, chemical kinetics, and polymer physics. J. Chem. Phys. **131**(22), 224902 (2009)
62. Stukalin, E.B., Cai, L.-H., Kumar, N.A., Leibler, L., Rubinstein, M.: Self-healing of unentangled polymer networks with reversible bonds. Macromolecules **46**(18), 7525–7541 (2013)
63. Frenkel, D., Smit, B.: Understanding molecular simulation: from algorithms to applications, vol. 1. Elsevier (2001)
64. Wilson, M., Rabinovitch, A., Baljon, A.R.C.: Computational study of the structure and rheological properties of self-associating polymer networks. Macromolecules **48**(17), 6313–6320 (2015). https://doi.org/10.1021/acs.macromol.5b00885
65. Simmons, D.S., Douglas, J.F.: Nature and interrelations of fast dynamic properties in a coarse-grained glass-forming polymer melt. Soft Matter **7**(22), 11010–11020 (2011)
66. Ma, C., Ji, T., Robertson, C.G., Rajeshbabu, R., Zhu, J., Dong, Y.: Effect of filler–polymer interface on elastic properties of polymer nanocomposites: a molecular dynamics study. Tire Sci. Technol. **45**(3), 227–241 (2017)
67. Khare, R., Paulaitis, M.E., Lustig, S.R.: Generation of glass structures for molecular simulations of polymers containing large monomer units: Application to polystyrene. Macromolecules **26**(26), 7203–7209 (1993)
68. Khabaz, F., Mani, S., Khare, R.: Molecular origins of dynamic coupling between water and hydrated polyacrylate gels. Macromolecules **49**(19), 7551–7562 (2016)
69. Todd, B.D., Daivis, P.J.: Nonequilibrium molecular dynamics: theory, algorithms and applications. Cambridge University Press (2017)

70. Edwards, B., Baig, C., Keffer, D.: A validation of the p-SLLOD equations of motion for homogeneous steady-state flows. J. Chem. Phys. **124**(19), 194104 (2006)
71. Meng, F., Pritchard, R.H., Terentjev, E.M.: Stress relaxation, dynamics, and plasticity of transient polymer networks. Macromolecules **49**(7), 2843–2852 (2016)
72. Meng, F., Saed, M.O., Terentjev, E.M.: Elasticity and relaxation in full and partial vitrimer networks. Macromolecules **52**, 7423–7429 (2019)
73. Treloar, L.R.G.: The physics of rubber elasticity (1975).
74. Kramers, H.A.: Brownian motion in a field of force and the diffusion model of chemical reactions. Phys. **7**(4), 284–304 (1940)
75. Doi, M.: Soft matter physics. Oxford University Press (2013)
76. Yu, K., Taynton, P., Zhang, W., Dunn, M.L., Qi, H.J.: Influence of stoichiometry on the glass transition and bond exchange reactions in epoxy thermoset polymers. RSC Adv. **4**(89), 48682–48690 (2014)
77. Green, M.S., Tobolsky, A.V.: A new approach to the theory of relaxing polymeric media. J. Chem. Phys. **14**(2), 80–92 (1946)
78. Smith, M.: ABAQUS/Standard User's Manual. Version **6**, 9 (2009)
79. Tobolsky, A.V.: Stress relaxation studies of the viscoelastic properties of polymers. J. Appl. Phys. **27**(7), 673–685 (1956). https://doi.org/10.1063/1.1722465
80. Sciortino, F.: Three-body potential for simulating bond swaps in molecular dynamics. Eur. Phys. J. E **40**, 3–6 (2017). https://doi.org/10.1140/epje/i2017-11496-5
81. Yu, K., Shi, Q., Li, H., Jabour, J., Yang, H., Dunn, M.L., Wang, T., Qi, H.J.: Interfacial welding of dynamic covalent network polymers. J. Mech. Phys. Solids **94**, 1–17 (2016). https://doi.org/10.1016/j.jmps.2016.03.009
82. Yu, K., Shi, Q., Wang, T., Dunn, M.L., Jerry Qi, H.: A computational model for surface welding in covalent adaptable networks using finite-element analysis. J. Appl. Mech. **83**(9), 091002 (2016). https://doi.org/10.1115/1.4033682
83. Vernerey, F.J., Long, R., Brighenti, R.: A statistically-based continuum theory for polymers with transient networks. J. Mech. Phys. Solids **107**, 1–20 (2017)